ACS APPLIED MATERIALS & INTERFACES

Research Article

www.acsami.org

Understanding Water Permeation in Graphene Oxide Membranes

Ning Wei,[†] Xinsheng Peng,[‡] and Zhiping Xu*[,†]

[†]Applied Mechanics Laboratory, Department of Engineering Mechanics and Center for Nano and Micro Mechanics, Tsinghua University, Beijing 100084, China

[‡]State Key Laboratory of Silicon Materials, Department of Materials Science and Engineering, Zhejiang University, Hangzhou 310028, China

ABSTRACT: Water transport through graphene-derived membranes has gained much interest recently due to its promising potential in filtration and separation applications. In this work, we explore water permeation in graphene oxide membranes using atomistic simulations and theoretical analysis, by considering flow through the interlayer gallery, expanded channels such as wrinkles of interedge spaces, and pores within the sheet. We find that, although flow enhancement can be established by nanoconfinement, fast water transport through pristine graphene channels is prohibited by a prominent side-pinning effect from capillaries formed within oxidized regions. We then discuss several flow enhancement mechanisms through the porous microstructures of graphene oxide membranes. These understandings are integrated into a complete picture to understand water permeation through the layer-by-layer and porous microstructure and can guide rational design of functional membranes for energy and environmental applications.

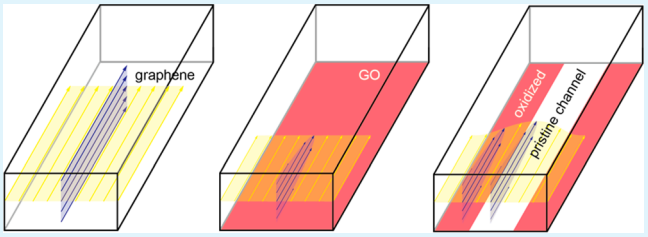

KEYWORDS: *graphene, graphene oxide, permeation, water transport, molecular dynamics*

INTRODUCTION

Graphene-derived functional membranes have recently been identified to be excellent candidate materials for filtration and separation applications because of their signature, although not well-characterized, porous microstructures.[1−12] Unimpeded permeation of water through submicrometer-thick graphene oxide (GO) membranes was observed with simultaneously completely impermeable performance for liquids, vapors, and gases including helium.[2] The unusually high water permeability was attributed to both capillary driven force and low-friction flow confined between two-dimensional channels of pristine graphene sheets.[2] On the other hand, we reported recently that nanostrand-channelled GO ultrafiltration membranes with a network of 3−5 nm nanochannels feature superior separation performance without sacrificing the rejection rate compared to unmodified GO membranes, because of their highly porous structure and significantly reduced channel length.[5] Ultrathin graphene nanofiltration membranes for water purification based on physical sieving and electrostatic interaction mechanisms were fabricated as well.[6]

In spite of the superior performance quantified in experiments and the emergence of promising applications, an understanding of the underlying filtration mechanism is still lacking, mainly due to the complexity in both microstructures and spatial distribution of chemical functional groups in the membrane (Figure 1). In this work, we explore water transport in GO membranes by performing atomistic simulations and continuum mechanics based analysis. We elucidate the viscous nature of water transport in GO. A prominent side-pinning effect is identified for water flow within the pristine graphene gallery sandwiched between oxidized regions in GO sheets, where flow enhancement is reduced by hydrogen bonds (H-bonds) between water molecules in the pristine and oxidized regions. This finding is in contradiction with the previously

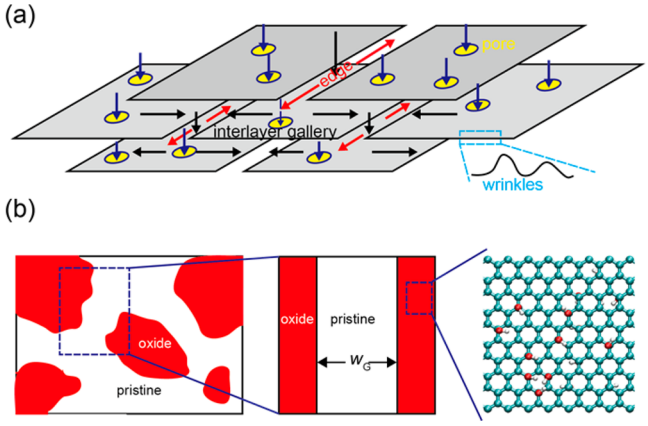

Figure 1. Microstructures of graphene-derived membranes. (a) The percolated water transport channel is composed of interlayer, interedge spaces, wrinkles, and pores (e.g., voids) within the graphene sheets. (b) The pristine and oxidized patterns on GO (left) are modeled in a quasi-2D molecular model (center) with oxygen-containing functionalization groups on both sides (right).

Received: February 5, 2014
Accepted: March 26, 2014
Published: March 26, 2014

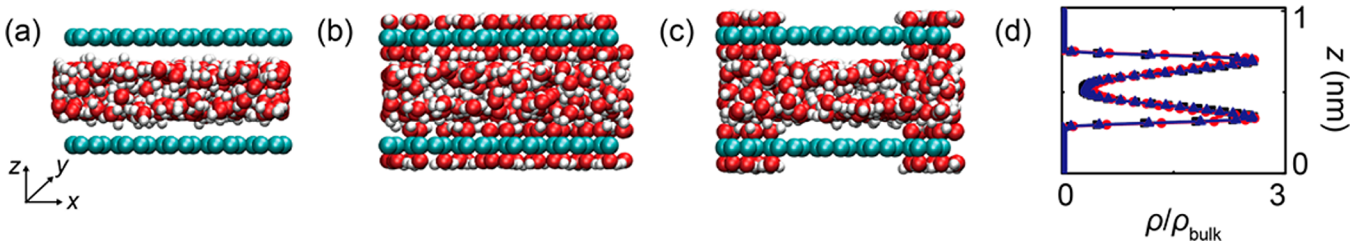

Figure 2. Atomic structures of water molecules confined between graphene and GO sheets. (a–c) Models constructed for water flow between graphene, GO with evenly distributed functional groups, and GO with patterned pristine and oxidized regions. Panel d shows density profiles along the thickness direction z, with filled squares for water between graphene sheets, dots for water between oxide regions in GO, and triangles for water between pristine regions in GO. ρ and ρ_{bulk} are the density of confined and bulk water, respectively.

proposed picture of fast water flow confined between pristine channels in GO membranes where the atomistically smooth graphitic surface leads to ultralow friction.[2,12] The reduced nanoconfinement effect measured directly from simulations corresponds to a low flow enhancement factor of ~1–10, and cannot explain the efficient water permeation through GO membranes, which may be attributed instead to the porous microstructures. Flow in several types of channels for water transport is then analyzed and discussed to manifest a complete picture for the permeation process.

MODELS AND METHODS

Atomic Structures. The molecular structure of GO consists of hydroxyl, epoxy, and carbonyl groups on the basal plane, as well as defective sites and open edges.[13−17] Hydroxyl groups were reported to be able to stay rich in the long-living quasi-equilibrium state[16] and thus are studied in this work, although our additional simulations show that epoxy groups have similar effects to the water flow.[18] A typical fraction of hydroxyl species relative to the amount of carbon atoms in GO is ~20%,[16] and further reduction could yield a lower concentration (13.9–15.9%) in the reduced graphene oxide (RGO).[19] For oxidized regions of GO, we construct hydroxyl-functionalized graphene on both sides of the sheet with concentration $c = n_{OH}/n_C = 20\%$ in this study, where n_{OH} and n_C are the number densities of hydroxyl groups and carbon atoms, respectively. The distribution of hydroxyl groups is sampled randomly in the oxidized region.

Interatomic Interaction Models and Molecular Dynamics Simulations. Classical molecular dynamics (MD) simulations are performed using the large-scale atomic/molecular massively parallel simulator (LAMMPS).[20] The all-atom optimized potential for liquid simulations (OPLS-AA) is used for GO, which can capture essential many-body terms in interatomic interactions, including bond stretching, bond angle bending, van der Waals, and electrostatic interactions.[21] This potential was successfully applied in studying pH-dependent behaviors of GO in aqueous solutions and compared consistently to experimental results.[21] Following previous studies on similar systems, the extended simple point charge model (SPC/E) is used for water molecules.[22,23] The SHAKE algorithm is applied for the stretching terms between oxygen and hydrogen atoms to reduce high-frequency vibrations that require shorter time steps. The interaction between water and GO includes both van der Waals and electrostatic terms. The former one is described by the 12–6 Lennard-Jones potential $4\varepsilon_{C-O}[(\sigma_{C-O}/r)^{12} - (\sigma_{C-O}/r)^6]$ between oxygen and carbon atoms with parameters $\varepsilon_{C-O} = 4.063$ meV and $\sigma_{C-O} = 0.319$ nm at an interatomic distance r.[24] The van der Waals forces are truncated at 1.0 nm, and the long-range Coulomb interactions are computed by using the particle–particle particle–mesh (PPPM) algorithm.[25] The channel length along the flow (y) direction is 12.3 nm, and the width (x) is 2.1 nm (Figure 2). Periodic boundary conditions (PBCs) are applied on all lateral directions. To ensure that the channel is fully filled by water at 1 atm and room temperature (300 K), we adjust the interlayer distance accordingly for specified content of water intercalation.[23]

The nature of nanoconfined flow depends critically on the liquid–solid interface.[18,23,26] One of the key parameters to characterize the interfacial interaction is the water contact angle (WCA). This above-mentioned set of simulation parameters predicts a WCA of $\theta_{c,G} = 98.4°$ for graphene in consistence with experimental measurement.[27] The WCA for GO, $\theta_{c,GO}$, is lower than $\theta_{c,G}$, and decreases with c. For example, for a typical value of $c = 20\%$ for GO, the simulation results in $\theta_{c,GO} = 26.8°$, which is also close to recent experimental measurements.[7,28] This consistence validates that the choices of OPLS-AA and SPC/E force fields and MD simulation parameters here offer reliable predictions for the water/GO hybrid system.[7]

Water Flow Simulations. The interfacial slip between water and graphene or GO is calculated through either the Green–Kubo formula in equilibrium molecular dynamics (EMD) or the definition of Navier slip length $L_s = v_s/(dv/dz)|_{z=0}$ in nonequilibrium molecular dynamics (NEMD), where v_s is the slip velocity at the fluid–wall interface and dv/dz is the tangent of the velocity profile along the normal direction z.[18] The position of the interface ($z = 0$) is defined as the averaged position of the first water layer, which is 0.35 nm away from the basal plane of graphene or GO sheets. Specifically in EMD, a friction coefficient λ can be calculated from the autocorrelation function of the time-dependence force acting on the surface and the slip length is defined accordingly as $L_s = \eta/\lambda$, where η is the viscosity.[29] In NEMD, the pressure-driven water flow is simulated by directly applying forces to water molecules, which results in a well-defined pressure gradient in the steady state. This nonequilibrium approach was widely used to explore nanoscale fluid transport, although the flow velocity is relatively higher than that under experimental conditions due to the limitation of length and time scales in MD simulations.[18,22,23] Our NEMD simulation results are further validated by their agreement with EMD results in the slip length, where no net flow or rate effect is present. The hybrid systems are first equilibrated at 300 K by using the Berendsen thermostat, where the temperature of fluid is calculated by excluding the center-of-mass motion. The carbon atoms in GO are constrained in the dynamic simulations to maintain the planar conformation of GO sheet as stacked in a paper or thin-film form. In GO samples, out-of-plane lattice distortion on the order of 0.1 nm can be induced by surface functionalization. However, our EMD simulation results show that the friction coefficient λ only increases ~3% by this lattice distortion effect, which is thus neglected in this work. Moreover, the wrinkled and crumpled morphologies of GO sheets at the micrometer scale are also not considered in this work because the typical size of pristine and oxidized regions is much more localized (~1–2 nm).[17,30−33] After the flow is driven, it usually takes a few nanoseconds to reach the steady flow state (1 ns for graphene, 3 ns for GO in this work), where the external driving and frictional forces balance and data is collected for our discussions below.

RESULTS

The characteristic microstructure of graphene-derived membranes is illustrated in Figure 1. The open path for water transport contains several types of channels that form a percolated network. In addition to cross-flow from pores (e.g., voids[33]) inside graphene sheets and interedge space between

neighboring sheets, the interlayer gallery may serve as a major channel considering the low porosity and edge-to-area ratio of graphene or GO sheets. This transverse flow path could reduce efficient water transport across the membrane if the channel density or connectivity is low enough. As a result, flow between GO sheets could be one of the major limiting factors in water permeation and is explored in this work.[2,5]

Water transport between graphene sheets was reported to feature remarkable boundary slip due to the diminishing friction at the liquid−solid interface, offering a remarkably high, curvature-dependent enhancement factor of ∼100−1000 compared to the nonslip viscous flow predictions, e.g., flow between parallel plates or inside tubes.[18,22,34] However, our recent work based on MD simulations shows that this ultrafast flow breaks down between hydrophilic oxidized graphene sheets due to the presence of oxygen-containing groups and their interaction with water molecules.[18] Layered water structures from monolayer, bilayers, to trilayers were identified for an interlayer distance d below 0.7, 1.0, and 1.4 nm, respectively, for both graphene and GO sheets. This value of d is in the typical range (0.7−1.2 nm) for GO immersed in water and increases with the water content, which agrees with recent measurements by Talyzin and co-workers.[35,36] Another interesting observation of the nanoconfined water structure is that the first water layer locates at the same distance from the pristine graphene and GO sheets, although the water−sheet interaction features a van der Waals nature in the former situation while H-bonds play a key role in GO.

Experimental and computational studies have shown that oxygen-containing groups tend to cluster in GO, forming patches of pristine and oxidized regions within the sheet, with typical sizes of 1−2 nm.[17,30−33] As GO is hydrophilic, while $\theta_{c,G}$ for graphene is in the neutral range 87−127°,[37] one could expect that, as a GO membrane is immersed into the solution and water molecules enter the interlayer gallery, they start by occupying hydrophilic oxidized regions and then open spaces between pristine regions. In a recent study, capillary driven flow and low-friction monolayer water transport within the pristine graphene channels were proposed to explain the unimpeded permeation of water through GO membranes, while oxidized regions were considered to act as spacers to separate GO with a certain interlayer distance for the capillary mechanism to work.[2] These arguments were made by assuming that water transport in the pristine channels still features significant enhancement as flow between graphene sheets. However, here we find in contrast that, although the water−graphene interface features low friction, the reduced water transport between oxidized regions around this pristine narrow 2D channel breaks down the expected flow enhancement. To show this effect, we perform MD simulations for model graphene and GO sheets. In addition to flow between graphene sheets (Figure 2a) and GO with evenly distributed functional groups (Figure 2b), a model with patterned GO is also studied, which consists of a straight, pristine graphene channel with width w_G = 1 nm, sandwiched between a neighboring oxidized region with width w_O = 1 nm (Figure 2c).[2,17] For all models, we set c = 20% for the oxidized regions and d = 1 nm if not specifically noted. The density profiles for water between graphene and patterned GO sheets are plotted along the thickness direction z in Figure 2d, which are almost coincident, indicating similar structures of water confined between pristine and oxidized regions in GO, and as a result identical fluid properties such as density and viscosity.

We then drive water flow by applying a pressure gradient along the channel direction. By plotting the velocity profiles across the channels, we find that, for flow between graphene, the low friction at the water−graphene interface leads to a flow velocity profile with very low curvature along the thickness direction z. The variance in velocity is less than 1% of its maximum amplitude and L_s is calculated to be 138 nm for d = 1 nm (Figure 3a). However, for water flow in pristine channels of

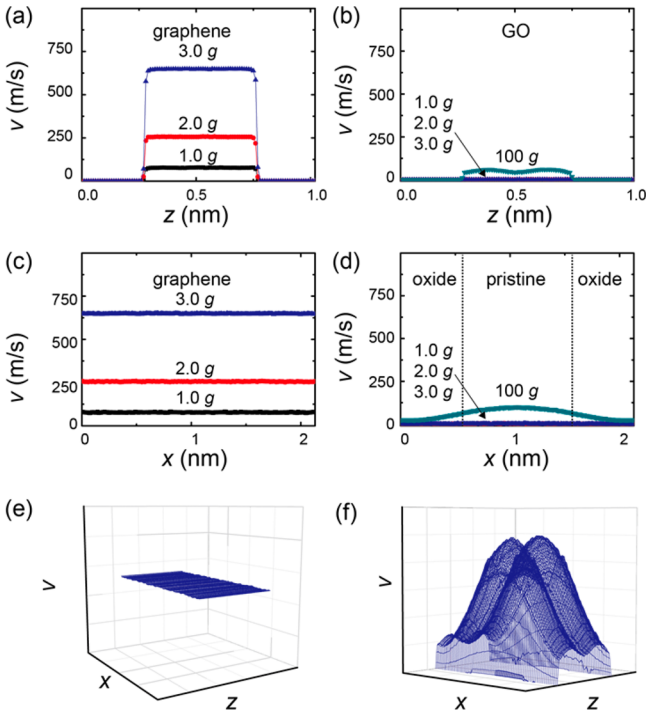

Figure 3. Velocity profiles for water flow between graphene and GO sheets: (a, c) for graphene and (b, d) for GO with patterned pristine and oxidized regions. The profiles are plotted along z (a, b) and x (c, d) directions, respectively. The flow profiles in three-dimensional space are also plotted in panels e and f schematically. The pressure gradient applied is g, $2g$, and $3g$ for data in panels a and c and g, $2g$, $3g$, and $100g$ for panels b and d, where g = 2.15 MPa/nm. It is distinct that, at the same pressure gradient, the velocity of water flow between GO sheets, even in the pristine region, is much reduced compared to that between graphene.

GO membranes, although a notable boundary slip still occurs between water and oxidized graphene (along the z direction, as shown in Figure 3b), contact with neighboring oxidized regions reduces flow speed at the interfaces (Figure 3d). This side-pinning effect leads to a high-curvature velocity profile with much reduced amplitude in the pristine region along the x direction (Figure 3d), in stark contrast to the flat one measured for flow between graphene sheets (Figure 3c). The slip length at this boundary between water in the pristine and oxidized regions L_s = 0.9 nm is very low (Figure 3d). That is to say, the presence of water capillary in neighboring oxidized regions impedes ultrafast water transport in 2D pristine graphene channels, in addition to their proposed role as spacers. This can be more distinctly seen from their three-dimensional velocity profiles plotted in Figure 3e and f as well as our schematic illustrations in Figure 4.

dx.doi.org/10.1021/am500777b | ACS Appl. Mater. Interfaces 2014, 6, 5877−5883

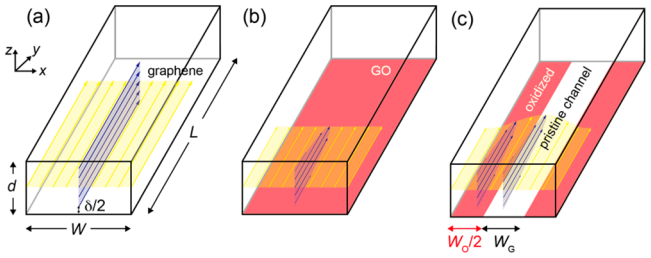

Figure 4. Schematic illustration of models for water flow between graphene or GO membranes. (a) Water flow between graphene sheets experiences significant boundary slip, and thus, the velocity profile is almost flat. (b) Flow between GO sheets is reduced compared to panel a, with a much shorter slip length. (c) Flow within the channel composed of pristine and oxidized graphene regions with widths w_G and w_O, respectively. The edge-pinning effect breaks down the ultrafast flow within the pristine channel. W, d, and L are the width, interlayer distance, and length of the flow channel, or the dimensions of the MD simulation box implemented with periodic boundary conditions. $\delta/2$ = 0.25 nm is the distance between water molecules and the graphene or GO sheets.

DISCUSSION

The well-characterized velocity profiles above allow us now to discuss the flow enhancement under experimental conditions more quantitatively. As illustrated in Figure 4, we now consider a nonslip Poiseuille flow confined between two flat plates separated by a distance d. The volumetric flux Q can be estimated as

$$Q_{\text{nonslip}} = -d^3\Delta PW/(12\eta L) \quad (1)$$

where d is the channel thickness that should be redefined here as the hydrodynamic thickness by excluding the vacuum space δ = 0.5 nm between water molecules and the graphene sheet, instead of the distance between basal planes of graphene or GO sheets. ΔP is the pressure difference across the channel with length L and width W, including both pristine and oxidized regions for GO. η is the apparent viscosity that can be calculated by fitting the velocity profiles by the Poiseuille one. The value of η usually differs from the bulk value due to changes in water structures under nanoconfinement.[18]

Water transport in nanochannels is usually enhanced compared to Q_{nonslip} because of significant boundary slip, which can be quantified by the flow enhancement factor ε through the slip length L_s as

$$\varepsilon = Q_{\text{slip}}/Q_{\text{nonslip}} = 1 + 6L_s/\delta \quad (2)$$

The values of L_s for graphene (Figure 4a) and GO with evenly distributed functional groups (Figure 4b) are calculated to be 138 and 0.2 nm from our MD simulations with a pressure gradient of 2.15 MPa/nm and interlayer distance of d = 1 nm, corresponding to ε_G = 1657 and ε_O = 3.7. These values of ε decrease with the interlayer distance. For d = 1.7 nm where layered water structure is not evident, our NEMD simulations show that ε is reduced to 227.5 for graphene and 3.4 for GO (Table 1).

Now we take into account the patterned nature of pristine and oxidized regions in GO. We first estimate the total flux through GO as a sum of contributions from pristine and oxidized regions, i.e.,

$$Q_{\text{GO}} = Q_G + Q_O = -\varepsilon_G\delta^3\Delta Pn_Gw_GW/(12\eta L) - \varepsilon_O\delta^3\Delta Pn_Ow_OW/(12\eta L) \quad (3)$$

Here we assume the model with infinite widths of pristine graphene and graphene oxide in parallel. A representative volume element consisting of one pristine and one oxidized channel is illustrated in Figure 4c. Q_G and Q_O are the flux measured through pristine and oxidized regions, and n_G (n_O), w_G(w_O), and ε_G (ε_O) are the number density of channels per width, channel width, and enhancement factor of pristine (oxidized) channels, respectively. By substituting the slip lengths calculated for graphene and GO with evenly distributed oxidized groups into eq 2, we find from eq 3 that the enhancement factor with respect to the nonslip Poiseuille prediction is $Q_{GO}/Q_{\text{nonslip}}$ = 830 for $w_G = w_O$ = 1 nm. This value is 2 orders higher than the actual value $Q_{MD}/Q_{\text{nonslip}}$ = 8.06, where Q_{MD} is the flux measured from our MD simulations. This inconsistence clearly indicates the aforementioned side-pinning effect on breaking down fast water transport through pristine graphene channels in GO membranes.

Our analysis on MD simulation results for the GO model shown in Figures 2c and 4c gives enhancement factors of ε_G = 11.81 and ε_O = 4.31 for water flow between pristine and oxidized regions, respectively. From these results for $w_G = w_O$ = 1 nm, some conclusions could be made on the basis of eq 3. As w_G increases, the enhancement factor ε_G for the pristine region increases from 11.81 to 1657 for $w_G = +\infty$. However, recent experimental and computational evidence suggests that the width of the pristine region is usually ~1−2 nm,[2,30−33] and ε_G thus should remain in the range 10−100. In contrast, ε_O decreases slightly with w_O, from ε_O = 4.31 for w_O = 1 nm to 3.7 for $w_O = +\infty$ in GO with evenly distributed oxidized groups. As a result, one can estimate water permeation from eq 3 using these simulated values of enhancement factors, as we will follow in the next paragraphs.

The GO membrane features rich channel microstructures in addition to the interlayer gallery as explored above, such as wide channels formed at wrinkles,[1,38] and open spaces between edges of neighboring GO sheets or platelets. These channels are much wider than the interlayer gallery, and could reach the scale of hundreds of nanometers or even micrometers. When considered in the analysis, there is additional flux by the amount of $Q_C = -\varepsilon_C\delta^3\Delta Pn_Cw_CW/(12\eta L)$, where n_C and w_C are the density and width of these additional channels. Q_C for wide channels could be responsible for high permeance measured in experiments, even without any flow enhancement, i.e., ε_C = 1. Due to the lack of detailed microstructural information on GO

Table 1. Summary of Simulation Parameters, Slip Lengths, and Enhancement Factors

	graphene (d = 1 nm)	graphene (d = 1.7 nm)	GO[a] (d = 1 nm)	GO[a] (d = 1.7 nm)	patterned GO (d = 1 nm, $w_G = w_O$ = 1 nm)
L_s (nm)	138	45.3	0.2	0.48	
ε	1657	227.5	3.7	3.4	8.06

[a]GO with evenly distributed oxygen-containing groups, c = 20%.

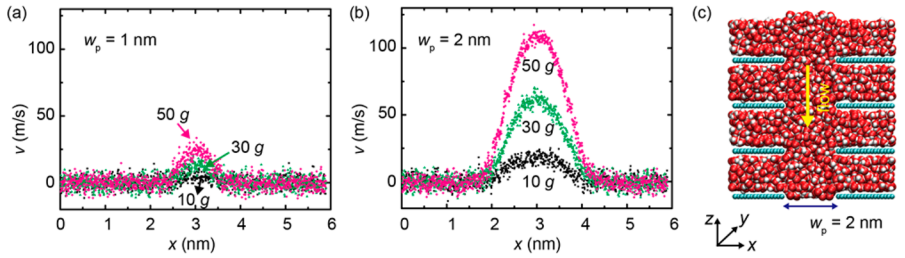

Figure 5. Velocity profiles for water transport within channels between graphene edges. The interedge distance is (a) 1 and (b) 2 nm, respectively. The pressure gradient applied is 10*g*, 30*g*, and 50*g*, where g = 2.15 MPa/nm. Panel c is a snapshot of the MD simulations.

membranes (e.g., sheet size, layer-by-layer stacking, distribution, corrugation), precise prediction cannot be made here. However, one could introduce an empirical prefactor p/τ, with porosity p and tortuosity τ fitted to experimentally measured permeability. Here tortuosity is the ratio between the average length of the fluid paths and the geometrical length of the sample. The permeability can be quantified by the ratio between the flow rate and pressure gradient. One of the implications of such enhancement by Q_C is that one can improve the permeability by creating wider nanochannels, as we have recently established through a nanostrand-templating approach.[5]

Recent work by Gao et al. showed that porous structures (e.g., voids) inside the GO sheet help flow enhancement as well.[6,33] We explore this effect by simulating flow along open graphene edges with an interedge distance w_p (Figure 5). The results suggest that the structure and viscosity of water within the channel are close to its bulk phase values, with a much weakened nanoconfinement effect compared to water in the interlayer gallery of the same spatial constriction. Notably, there is no apparent boundary slip, and thus for pores within graphene or GO sheets, the permeance will not be significant for a size of a few nanometers. From our MD simulation results (Figure 5), the estimated ratio R between flux Q and the pressure gradient $-\Delta P/L$ is 2.16×10^{-13} and 3.02×10^{-12} L(MPa/nm)$^{-1}$ h^{-1} for w_p = 1 and 2 nm, respectively. We compare the result at w_p = 2 nm with the results for water flow between GO or graphene sheets at d = 2 nm, where the water structure is close to that in the bulk phase. Our MD simulations show that $R_{GO} = 7.56 \times 10^{-12}$ L(MPa/nm)$^{-1}$ h^{-1} for GO with evenly distributed functional groups and $R_G = 4.56 \times 10^{-10}$ L(MPa/nm)$^{-1}$ h^{-1} for graphene. Thus, at the same nanoconstriction, the permeability of interedge flow is close to the flow between oxidized graphene but is significantly reduced compared with flow between pristine graphene sheets. Moreover, by considering the random distribution of pores in the graphene, the probability for a water molecule to pass through an N-layer membrane with pore size a_p and density n_p decreases with N as $2(a_p n_p)^{N-1}$. As a result, this effect shortens the transport path but is only significant for ultrathin membranes. For example, the thickness of GO membranes is 22−53 nm in Gao et al. experiments.[6] A similar argument should hold for gas separation membranes where diffusive motion of gas molecules drives the transport across membranes, although the lack of cooperative H-bonds and reduced density in the gas phase would modify the nature of flow therein.[8,9] Following these findings, one could further improve the permeability by using graphene sheets with smaller size for a higher density of interedge spaces, or introducing wider channels, although the structural integrity and mechanical stability should be well maintained in these engineered membranes.[39]

According to the elucidated physical picture of interlayer gallery flow and eq 3, we find that the overall flow enhancement factor ε is only on the order of 10 for typical length scales of the pristine and oxidized regions in GO, e.g., ε = 8.06 for $w_G = w_O$ = 1 nm (Table 1). Although our additional MD simulations show that ε increases with w_G and could reach 98.18 for w_G = 4 nm and w_O = 1 nm, the experimental evidence that w_G ∼1−2 nm cannot support the explanation of high permeability by these pristine channels.[2,30−33] Moreover, the pristine and oxidized regions in GO are discretely distributed[2,30−33] rather than lining up even if a percolated network could form, so the straight channel picture could break down, which leads to an even lower interlayer flow rate. As a result, the measurement of water permeation made recently[2] reporting enhancement factors of tens to hundreds, driven by $-\Delta P$ = 23 mbar (after excluding the capillary pressure ∼1−10 kbar) across a channel of ∼1 μm, may arise from wider channels or interedge spaces in the membrane.

CONCLUSION

On the basis of discussions above, we conclude here that the reported fast flow of water across graphene-derived membranes may be attributed majorly to their porous microstructures (e.g., expanded interlayer gallery, wide channels formed at wrinkles, holes, and interedge spaces), followed by the less significant enhancement by boundary slip. The physical picture of ultrafast flow between pristine graphene sheets breaks down due to a side-pinning effect by water confined between oxidized regions in GO membranes. By using adjusted density and viscosity for nanoconfined water, the interfacial slip length directly calculated from MD simulations, or the enhancement factor they lead to, one could calculate the permeability from a continuum viscous model. These understandings not only lay the groundwork for future design of high-performance membranes for filtration and separation applications but can also be extended to other membranes with similar layered microstructures, such as those constructed from MoS_2 sheets, WS_2 sheets, or their hybrids,[40] although a detailed characterization of their microstructures is required to allow quantitative prediction. Moreover, one could design separation membranes for species with contrastive strength of the pinning effect, which depends on the strength of van der Waals forces, H-bonds with the species, as well as the density of species and interlayer separation of the GO membrane. For example, transport of nonpolar gases such as H_2 may be unimpeded due to its weak interaction with GO and low density.

AUTHOR INFORMATION

Corresponding Author

*E-mail: xuzp@tsinghua.edu.cn.

Notes

The authors declare no competing financial interest.

ACKNOWLEDGMENTS

This work was supported by the National Natural Science Foundation of China through grants 11222217, 11002079, and 21271154, Tsinghua University Initiative Scientific Research Program 2011Z02174, and the Postdoctoral Science Foundation of China 023220045. The computer simulations were performed on the Explorer 100 cluster system of Tsinghua National Laboratory for Information Science and Technology.

REFERENCES

(1) Qiu, L.; Zhang, X.; Yang, W.; Wang, Y.; Simon, G. P.; Li, D. Controllable Corrugation of Chemically Converted Graphene Sheets in Water and Potential Application for Nanofiltration. *Chem. Commun.* **2011**, *47*, 5810−5812.

(2) Nair, R. R.; Wu, H. A.; Jayaram, P. N.; Grigorieva, I. V.; Geim, A. K. Unimpeded Permeation of Water through Helium-Leak-Tight Graphene-Based Membranes. *Science* **2012**, *335*, 442−444.

(3) Raidongia, K.; Huang, J. Nanofluidic Ion Transport through Reconstructed Layered Materials. *J. Am. Chem. Soc.* **2012**, *134*, 16528−16531.

(4) Huang, H.; Mao, Y.; Ying, Y.; Liu, Y.; Sun, L.; Peng, X. Salt Concentration, Ph and Pressure Controlled Separation of Small Molecules through Lamellar Graphene Oxide Membranes. *Chem. Commun.* **2013**, *49*, 5963−5965.

(5) Huang, H.; Song, Z.; Wei, N.; Shi, L.; Mao, Y.; Ying, Y.; Sun, L.; Xu, Z.; Peng, X. Ultrafast Viscous Water Flow through Nanostrand-Channelled Graphene Oxide Membranes. *Nat. Commun.* **2013**, *4*, 3979.

(6) Han, Y.; Xu, Z.; Gao, C. Ultrathin Graphene Nanofiltration Membrane for Water Purification. *Adv. Funct. Mater.* **2013**, *23*, 3693−3700.

(7) Sun, P.; Zhu, M.; Wang, K.; Zhong, M.; Wei, J.; Wu, D.; Xu, Z.; Zhu, H. Selective Ion Penetration of Graphene Oxide Membranes. *ACS Nano* **2013**, *7*, 428−437.

(8) Kim, H. W.; Yoon, H. W.; Yoon, S.-M.; Yoo, B. M.; Ahn, B. K.; Cho, Y. H.; Shin, H. J.; Yang, H.; Paik, U.; Kwon, S.; Choi, J.-Y.; Park, H. B. Selective Gas Transport through Few-Layered Graphene and Graphene Oxide Membranes. *Science* **2013**, *342*, 91−95.

(9) Li, H.; Song, Z.; Zhang, X.; Huang, Y.; Li, S.; Mao, Y.; Ploehn, H. J.; Bao, Y.; Yu, M. Ultrathin, Molecular-Sieving Graphene Oxide Membranes for Selective Hydrogen Separation. *Science* **2013**, *342*, 95−98.

(10) Sun, P.; Zheng, F.; Zhu, M.; Song, Z.; Wang, K.; Zhong, M.; Wu, D.; Little, R. B.; Xu, Z.; Zhu, H. Selective Trans-Membrane Transport of Alkali and Alkaline Earth Cations through Graphene Oxide Membranes Based on Cation−Π Interactions. *ACS Nano* **2014**, *8*, 850−859.

(11) Joshi, R. K.; Carbone, P.; Wang, F. C.; Kravets, V. G.; Su, Y.; Grigorieva, I. V.; Wu, H. A.; Geim, A. K.; Nair, R. R. Precise and Ultrafast Molecular Sieving through Graphene Oxide Membranes. *Science* **2014**, *343*, 752−754.

(12) Mi, B. Graphene Oxide Membranes for Ionic and Molecular Sieving. *Science* **2014**, *343*, 740−742.

(13) Lerf, A.; He, H.; Forster, M.; Klinowski, J. Structure of Graphite Oxide Revisited. *J. Phys. Chem. B* **1998**, *102*, 4477−4482.

(14) Gao, W.; Alemany, L. B.; Ci, L.; Ajayan, P. M. New Insights into the Structure and Reduction of Graphite Oxide. *Nat. Chem.* **2009**, *1*, 403−408.

(15) Bagri, A.; Mattevi, C.; Acik, M.; Chabal, Y. J.; Chhowalla, M.; Shenoy, V. B. Structural Evolution During the Reduction of Chemically Derived Graphene Oxide. *Nat. Chem.* **2010**, *2*, 581−587.

(16) Kim, S.; Zhou, S.; Hu, Y.; Acik, M.; Chabal, Y. J.; Berger, C.; de Heer, W.; Bongiorno, A.; Riedo, E. Room-Temperature Metastability of Multilayer Graphene Oxide Films. *Nat. Mater.* **2012**, *11*, 544−549.

(17) Kumar, P. V.; Bardhan, N. M.; Tongay, S.; Wu, J.; Belcher, A. M.; Grossman, J. C. Scalable Enhancement of Graphene Oxide Properties by Thermally Driven Phase Transformation. *Nat. Chem.* **2013**, *6*, 151−158.

(18) Wei, N.; Peng, X.; Xu, Z. Breakdown of Fast Water Transport in Graphene Oxides. *Phys. Rev. E* **2014**, *89*, 012113.

(19) Dreyer, D. R.; Park, S.; Bielawski, C. W.; Ruoff, R. S. The Chemistry of Graphene Oxide. *Chem. Soc. Rev.* **2010**, *39*, 228−240.

(20) Plimpton, S. Fast Parallel Algorithms for Short-Range Molecular Dynamics. *J. Comp. Phys.* **1995**, *117*, 1−19.

(21) Shih, C.-J.; Lin, S.; Sharma, R.; Strano, M. S.; Blankschtein, D. Understanding the Ph-Dependent Behavior of Graphene Oxide Aqueous Solutions: A Comparative Experimental and Molecular Dynamics Simulation Study. *Langmuir* **2011**, *28*, 235−241.

(22) Falk, K.; Sedlmeier, F.; Joly, L.; Netz, R. R.; Bocquet, L. Molecular Origin of Fast Water Transport in Carbon Nanotube Membranes: Superlubricity Versus Curvature Dependent Friction. *Nano Lett.* **2010**, *10*, 4067−4073.

(23) Xiong, W.; Liu, J. Z.; Ma, M.; Xu, Z.; Sheridan, J.; Zheng, Q. Strain Engineering Water Transport in Graphene Nanochannels. *Phys. Rev. E* **2011**, *84*, 056329.

(24) Werder, T.; Walther, J. H.; Jaffe, R. L.; Halicioglu, T.; Koumoutsakos, P. On the Water-Carbon Interaction for Use in Molecular Dynamics Simulations of Graphite and Carbon Nanotubes. *J. Phys. Chem. B* **2003**, *107*, 1345−1352.

(25) Hockney, R. W.; Eastwood, J. W. *Computer Simulation Using Particles*; Taylor & Francis: 1989.

(26) Thomas, J. A.; McGaughey, A. J. H. Reassessing Fast Water Transport through Carbon Nanotubes. *Nano Lett.* **2008**, *8*, 2788−2793.

(27) Rafiee, J.; Mi, X.; Gullapalli, H.; Thomas, A. V.; Yavari, F.; Shi, Y.; Ajayan, P. M.; Koratkar, N. A. Wetting Transparency of Graphene. *Nat. Mater.* **2012**, *11*, 217−222.

(28) Wei, N.; Lv, C.; Xu, Z. Wetting of Graphene Oxide: A Molecular Dynamics Study. *Langmuir* **2014**, *30*, 3572−3578.

(29) Bocquet, L. r.; Barrat, J.-L. Hydrodynamic Boundary Conditions, Correlation Functions, and Kubo Relations for Confined Fluids. *Phys. Rev. E* **1994**, *49*, 3079−3092.

(30) Zhou, S.; Bongiorno, A. Origin of the Chemical and Kinetic Stability of Graphene Oxide. *Sci. Rep.* **2013**, *3*, 2484.

(31) Wilson, N. R.; Pandey, P. A.; Beanland, R.; Young, R. J.; Kinloch, I. A.; Gong, L.; Liu, Z.; Suenaga, K.; Rourke, J. P.; York, S. J.; Sloan, J. Graphene Oxide: Structural Analysis and Application as a Highly Transparent Support for Electron Microscopy. *ACS Nano* **2009**, *3*, 2547−2556.

(32) Pacilé, D.; Meyer, J. C.; Fraile Rodríguez, A.; Papagno, M.; Gómez-Navarro, C.; Sundaram, R. S.; Burghard, M.; Kern, K.; Carbone, C.; Kaiser, U. Electronic Properties and Atomic Structure of Graphene Oxide Membranes. *Carbon* **2011**, *49*, 966−972.

(33) Erickson, K.; Erni, R.; Lee, Z.; Alem, N.; Gannett, W.; Zettl, A. Determination of the Local Chemical Structure of Graphene Oxide and Reduced Graphene Oxide. *Adv. Mater.* **2010**, *22*, 4467−4472.

(34) Thomas, J. A.; McGaughey, A. J. H. Water Flow in Carbon Nanotubes: Transition to Subcontinuum Transport. *Phys. Rev. Lett.* **2009**, *102*, 184502.

(35) Talyzin, A. V.; Hausmaninger, T.; You, S.; Szabo, T. The Structure of Graphene Oxide Membranes in Liquid Water, Ethanol and Water-Ethanol Mixtures. *Nanoscale* **2014**, *6*, 272−281.

(36) Talyzin, A. V.; Luzan, S. M.; Szabó, T.; Chernyshev, D.; Dmitriev, V. Temperature Dependent Structural Breathing of Hydrated Graphite Oxide in H_2O. *Carbon* **2011**, *49*, 1894−1899.

(37) Taherian, F.; Marcon, V.; van der Vegt, N. F. A.; Leroy, F. What Is the Contact Angle of Water on Graphene? *Langmuir* **2013**, *29*, 1457−1465.

(38) Najmaei, S.; Liu, Z.; Zhou, W.; Zou, X.; Shi, G.; Lei, S.; Yakobson, B. I.; Idrobo, J.-C.; Ajayan, P. M.; Lou, J. Vapour Phase

Growth and Grain Boundary Structure of Molybdenum Disulphide Atomic Layers. *Nat. Mater.* **2013**, *12*, 754−759.
(39) Liu, Y.; Xie, B.; Zhang, Z.; Zheng, Q.; Xu, Z. Mechanical Properties of Graphene Papers. *J. Mech. Phys. Solids* **2012**, *60*, 591−605.
(40) Sun, L.; Huang, H.; Peng, X. Laminar MoS_2 Membranes for Molecule Separation. *Chem. Commun.* **2013**, *49*, 10718−10720.